ARTICLE

Electron Paramagnetic Resonance Investigation of Purified Catalyst-free Single-Walled Carbon Nanotubes

Mujtaba Zaka,[†] Yasuhiro Ito,[†] Huiliang Wang,[†] Wenjing Yan,[†] Alex Robertson,[†] Yimin A. Wu,[†] Mark H. Rümmeli,[‡,§] David Staunton,[⊥] Takeshi Hashimoto,[¶] John J. L. Morton,[†] Arzhang Ardavan,[#] G. Andrew D. Briggs,[†] and Jamie H. Warner[†,*]

[†]Department of Materials, University of Oxford, Parks Rd, Oxford, OX1 3PH, United Kingdom, [‡]IFW Dresden, P.O. Box 270116, D-01171 Dresden, Germany, [§]Technische Universität Dresden, Dresden, D-01062, Germany, [⊥]Department of Biochemistry, University of Oxford, South Parks Road, Oxford, OX1 3QU, United Kingdom, [¶]Meijo Nano Carbon Co. Ltd, 3-4-10 Marunouchi, Naka-ku, Nagoya, 460-0002, Japan, and [#]Clarendon Laboratory, Department of Physics, University of Oxford, Parks Rd, Oxford, OX1 3PH, United Kingdom

ABSTRACT Electron paramagnetic resonance of single-walled carbon nanotubes (SWCNTs) has been bedevilled by the presence of paramagnetic impurities. To address this, SWCNTs produced by laser ablation with a nonmagnetic PtRhRe catalyst were purified through a multiple step centrifugation process in order to remove amorphous carbon and catalyst impurities. Centrifugation of a SWCNT solution resulted in sedimentation of carbon nanotube bundles containing clusters of catalyst particles, while isolated nanotubes with reduced catalyst particle content remained in the supernatant. Further ultracentrifugation resulted in highly purified SWCNT samples with a narrow diameter distribution and almost no detectable catalyst particles. Electron paramagnetic resonance (EPR) signals were detected only for samples which contained catalyst particles, with the ultracentrifuged SWCNTs showing no EPR signal at X-band (9.4 GHz) and fields < 0.4 T.

KEYWORDS: single-walled · nanotubes · electron paramagnetic resonance · ultracentrifugation

Carbon nanotubes are ideal for the production of spintronic[1] devices owing to the long electron spin lifetimes and high Fermi velocity.[2] It is vital to understand the magnetic properties of electrons in single-walled carbon nanotubes (SWCNTs) in order to effectively utilize them in spintronics. Electron paramagnetic resonance (EPR) is an ideal method for providing insights into the spin properties of SWCNTs as it can probe conduction electrons and unpaired spins. EPR of SWCNTs was reported by Petit *et al.*,[3] and a strong signal attributed to conduction electrons was observed. Bandow *et al.*[4] reported experiments on multiwalled nanotubes and SWCNTs that indicated a relationship between contacting nanotube bundles and the EPR line shape. Contrary to the experiment by Petit, no signal associated with the presence of conduction electrons was detected. Salvetat[5] irradiated SWCNTs with 2.5 MeV electrons, inducing defects, in order to detect conduction electron spin resonance. However, the EPR spectrum was dominated by magnetic catalyst impurities. In an attempt to solve this problem of magnetic catalyst particle impurities Corzilius *et al.*[6] used carbon nanotubes grown using chemical vapor deposition (CVD). These vertically aligned forests of nanotubes can be removed from the substrate, leaving behind the residual catalyst. Low temperature measurements found sharp EPR lines that were attributed to conduction electrons trapped inside nanotube defects. However, the lack of in-depth structural characterization by high resolution transmission electron microscopy (HRTEM) makes it difficult to link EPR properties with specific structural features of the SWCNTs. EPR has also been employed to study SWCNT peapod structures[7,8] elucidating charge transfer between metallofullerenes and SWCNTs, and hydrogen absorption[9] of nanotubes preferentially at defect sites, causing the EPR signal to diminish.

These often discordant results of SWCNT EPR highlight the need for ultrapure samples free from metal impurities and the application of multiple characterization techniques in order to build a balanced and deep picture of the structure−EPR relationship. SWCNTs have generally been grown using magnetic transition metal catalyst particles,[3−5] which contribute strong EPR signals, and efforts to remove magnetic particles often leave the SWCNTs highly defective.[6] Preparation of high quality pristine SWCNTs are essential for the investigation of the origin of SWCNT EPR. SWCNTs processing requires the removal

*Address correspondence to Jamie.warner@materials.ox.ac.uk.

Received for review September 30, 2010 and accepted November 2, 2010.

Published online November 17, 2010. 10.1021/nn102602a

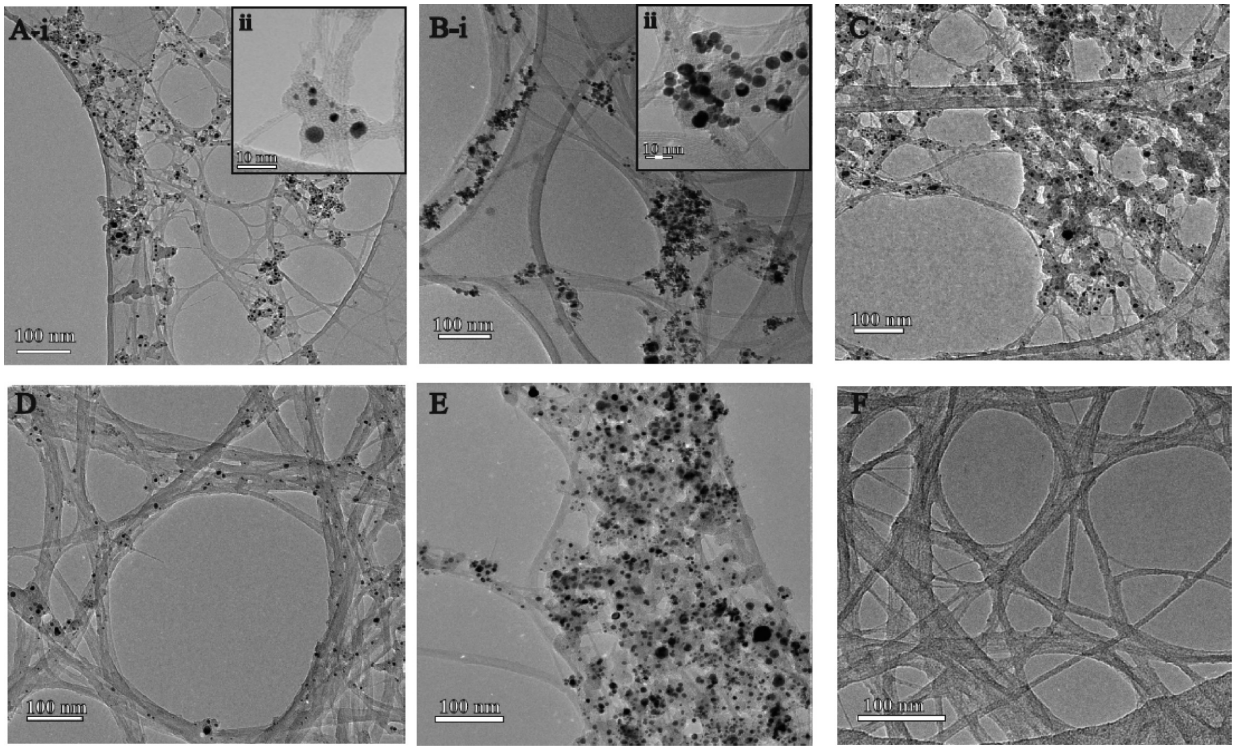

Figure 1. HRTEM images illustrating the composition of the SWCNT samples through each step in the purification process: (A-i) low-magnification image of raw laser ablation PtRhRe SWCNTs; (A-ii) high-magnification image of raw SWCNTs showing amorphous carbon coating the nanotube surface; (B-i) low-magnification image of annealed PtRhRe SWCNTs; (B-ii) high-magnification image of annealed SWCNTs showing clean nanotubes and catalyst particles; (C) sonicated PtRhRe SWCNTs coated with surfactant; (D) centrifuged SWCNT supernatant showing a reduction in catalyst particles; (E) low-magnification image of centrifuged SWCNT sediment showing large clusters of catalyst particles; (F) HRTEM image of DGU treated SWCNTs showing minimal catalyst particle content.

of amorphous carbon and catalyst particles with minimal damage to the nanotube structure.

Here, we utilize two different purification methods to remove amorphous and graphitic carbon, and catalyst particle impurities, based upon high vacuum high thermal annealing and ultracentrifugation.[10,11] Kitaura *et al.*[10] annealed raw SWCNTs at 1200 °C for 24 h under high vacuum to remove amorphous carbon and vaporize Fe catalyst particles. Superconducting quantum interference device (SQUID) magnetometry of the thermally annealed SWCNT sample showed minimal magnetic susceptibility over the temperature range, demonstrating the removal of Fe catalyst particles while retaining nanotube structure. Ultracentrifugation allows for facile separation of nanotubes and catalyst particles without damaging the carbon nanotube structure. Density gradient ultracentrifugation (DGU) has been developed as a large scale method for the separation of SWCNTs into semiconducting and metallic chiralities, primarily focusing on smaller diameter nanotubes.[12,13] Larger diameter SWCNTs are more challenging to separate into different chiral forms due to the broad overlap of diameter for semiconducting and metallic species. We have concentrated on larger diameter SWCNTs because they can be filled with spin-active metallofullerenes to form 1D peapod systems.[7]

RESULTS AND DISCUSSION

Nanotube Composition. HRTEM was performed to image the composition of all SWCNT samples in each of the purification methods, comparing the nanotube structure and the level of catalyst particles, amorphous carbon and defects present. Figure 1 panels a-i and a-ii show the HRTEM images from the raw PtRhRe SWCNTs containing catalyst particles, amorphous and graphitic carbon. The SWCNTs were annealed in air at 300 °C for 2 h to remove the carbon impurities. Figure 1 panels b-i and b-ii show the annealed PtRhRe SWCNTs with reduced amounts of amorphous carbon either on the surface of the nanotube or surrounding the catalyst particles. A solution of annealed SWCNTs in 2% SC/DOC [4:1 ratio] was prepared and then sonicated for 4 h. HRTEM presented in Figure 1c shows SWCNTs and catalyst particles coated with surfactant. The sonicated SWCNT sample was centrifuged for 1 h at 41 krpm, resulting in the supernatant (top 85%) containing dilute SWCNT solution with the bottom containing a residue of sediment SWCNTs. The "supernatant SWCNT", Figure 1D, shows a reduction in the amount of catalyst particles and more isolated SWCNTs. In contrast, Figure 1E, the "sediment SWCNT" sample, showed considerable increase in the level of catalyst particles. The supernatant SWCNT sample was further purified through a 17 h ultracentrifugation using a 20−40% iodixanol density gradient based upon the DGU method explained in ref

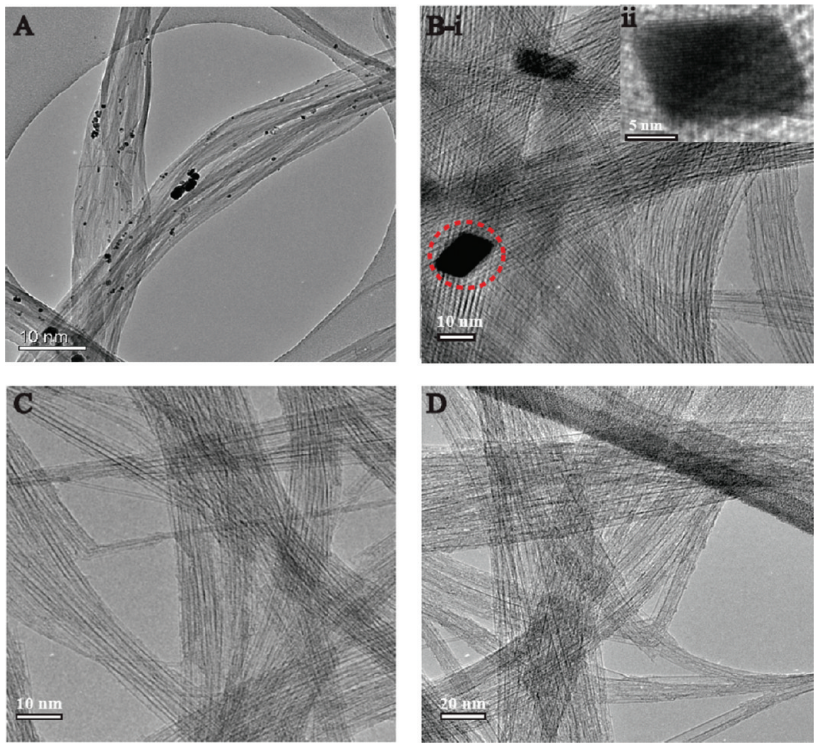

Figure 2. (A) Low-magnification HRTEM image of aqua regia treated SWCNTs showing clean nanotube bundle with some catalyst particles; (B-i) HRTEM image of Meijo SO SWCNTs showing a residual catalyst particle, highlighted with dotted circle; (B-ii) high magnification HRTEM of highlighted catalyst particle showing lattice fringes; (C) low-magnification HRTEM image of large bundles of Meijo FHP NTs with no visible catalyst particles; (D) HRTEM image of Meijo FHP NTs refluxed in HNO_3, showing bundles of NTs maintaining pristine structure.

12. The resulting sample, Figure 1F, contains many isolated SWCNTs with almost no visible catalyst particles. The centrifuge purification process has been developed as an alternative method to the currently employed aqua regia purification method.[7,14,15] Aqua regia involves harsh acid treatment to remove the catalyst particles, but, as shown in Figure 2a, a significant amount of catalyst particles remains. Hot thermal annealing has been previously employed as a purification method for arc-discharge nanotubes.[16] HRTEM of Meijo SO SWCNTs, shown in Figure 2b, indicates the presence of some residual catalyst particles. Figure 2c shows the HRTEM image of Meijo FHP CNTs with a combination of single-walled and double-walled nanotubes and almost no magnetic catalyst particles. Several hours were spent using TEM to scan a region of more than 0.01 mm^2 of FH-P SWNT networks that was found to be catalyst free. The Meijo FHP NTs were refluxed in HNO_3 for 2.5 h in order to produce defects;[17] Figure 2d shows the refluxed Meijo FHP sample still retaining its nanotube structure and no magnetic particles visible.

Purity Analysis Using Absorption Spectroscopy. Van-Hove singularities in SWCNTs produce distinctive absorption peaks from semiconducting and metallic transitions. UV−vis absorption spectroscopy was used to measure the absorption peaks from the metallic and semiconducting SWCNTs and yield information regarding the diameter distribution and purity of SWCNTs in the ultracentrifugation purification process. UV−vis absorption of SWCNT films between 400−2200 nm showed two semiconducting peaks, around S_{11} = 1900 nm and S_{22} = 1050 nm, and the first metallic peak, around M_{11} = 700 nm (see Supporting Information). For comparative analysis, the full width half-maximum (fwhm) diameter distribution, calculated using Kataura plot,[18] and the relative purity obtained from the S_{22} peak was examined for all samples (shown in Figure 3a). The mean diameter remained consistent, approximately ~1.45 nm, for all SWCNT samples in the purification process. The SWCNT sediment has the broadest fwhm diameter distribution, shown in Figure 3b, while the SWCNT supernatant and DGU SWCNT material have narrower fwhm diameter distribution. Surprisingly the SWCNT sediment and sonicated SWCNT contain narrow nanotubes with diameters < 1.2 nm. These narrow diameter nanotubes may bundle together and cause them to sediment. Centrifugation of SWCNT solutions should force heavy nanotube bundles to sediment, and isolated nanotubes to form in the supernatant. SWCNT purity is a measure of the absorption of SWCNT against impurities in the sample as explained in ref 19. Relative to the sonicated SWCNT sample the purity increases for the centrifuged supernatant and DGU SWCNT sample, which has the highest relative purity. The sediment SWCNT sample has the lowest relative purity, which is reflective of the high levels of catalyst particles as illustrated in the HRTEM, Figure 1E. Meijo FHP CNTs produced a broad UV−vis absorption spectra due to a very large diameter distribution, therefore a fwhm and purity could not be determined.

Structural Analysis. Atomic force microscopy (AFM) provided a further insight into the affect of the centrifugation purification process on the length and bundling of the PtRhRe SWCNTs. HRTEM only provides a qualitative idea of the length distribution of the SWCNTs samples, so it is important to use AFM as an additional analytical technique. AFM of raw PtRhRe SWCNT, centrifuged SWCNT supernatant, and Meijo FHP SWCNT are shown in Figure 4 panels a, b, and c, respectively, and analyzed in Figure 4d,e. All samples were prepared in 2% SC/DOC [4:1 ratio] solution and to ensure good dispersions raw PtRhRe SWCNTs and Meijo FHP CNTs were sonicated for 1 h. Raw PtRhRe SWCNTs have a mean length of 1.41 μm and the majority of nanotubes with length between 1 and 2 μm. For the SWCNT supernatant the distribution of nanotube lengths peaks at 0.5−1 μm with an average nanotube length of 0.77 μm. The shorter nanotube length is due to the 4 h horn-

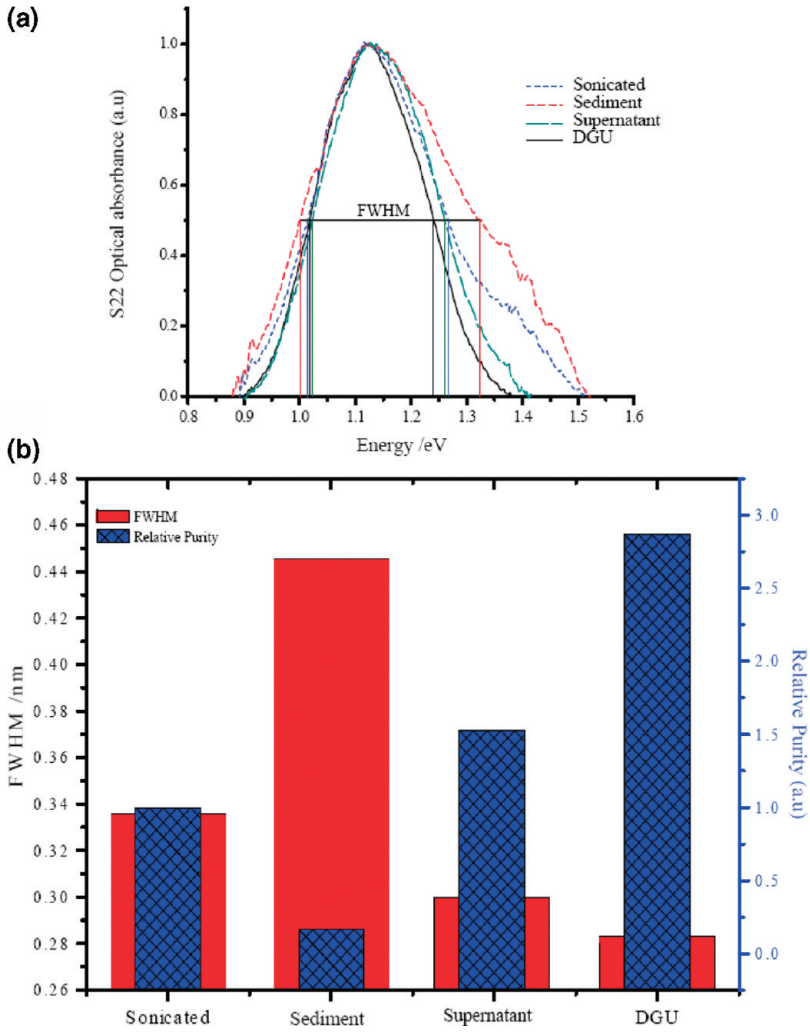

Figure 3. (a) UV−vis absorption showing the normalized S_{22} peak for the SWCNTs sample, indicating the fwhm for each sample; (b) fwhm diameter distribution (red) and relative purity (blue) relative to sonicated SWCNTs sample for SWCNTs samples, with the S_{22} peak used as a comparison for all samples.

tip sonication of the nanotube which is known to cut and shorten SWCNTs.[20,21] The height profile distribution for raw PtRhRe peaks between 2 and 4 nm (*i.e.*, bundles), compared to the lower value of the SWCNTs supernatant, with the majority of the height profile distribution less than 2 nm. This indicates that the SWCNT supernatant contains principally isolated nanotubes, which is a direct result of the surfactant encapsulation and centrifugation of the SWCNT. Meijo FHP CNTs are much shorter in length than Raw PtRhRe SWCNTs, with a mean length of 0.57 μm. Meijo FHP CNTs have a larger height profile distribution compared to raw PtRhRe SWCNT, due to the larger diameter of the Meijo FHP CNTs and the presence of both single-walled and double-walled nanotubes. AFM data indicate that both supernatant SWCNTs and Meijo FHP NTs have sufficient mean length to produce isolated NT field effect transistor (FET) devices as explained in ref 22. Percolated networks of short NTs, ~200 nm mean length, have been employed to produce thin film transistors.[23]

Electron Paramagnetic Resonance. X-Band CW EPR measurements for each of the SWCNT species in the centrifugation purification process were performed at 5 K using microwave power of ~1 mW (well below the saturation power of ~2 mW). EPR samples were prepared with a similar quantity of SWCNTs in order to compare the relative number of spins. Figure 5 compares the EPR intensity of the various SWCNT samples. Raw PtRhRe SWCNTs, Figure 5a, gave a strong single peak in the EPR, with a *g*-factor of 2.0034 ± 0.0005 and line width ≈ 3.0 ± 0.1 G, but when the SWCNTs were annealed this signal was no longer detected. We attribute this loss of EPR signal to the removal of amorphous carbon in the annealing process. Centrifugation of the sonicated PtRhRe SWCNT sample decreased the catalyst content and improved the purity of the SWCNT supernatant sample compared to the SWCNTs sediment. The sonicated and sedimented SWCNT samples show an EPR signal, Figure 5b, with a Lorentzian line shape and similar linewidths of ~5.0 ± 0.1 G. The *g*-factor for sonicated and sediment SWCNTs are 2.0029 ± 0.0005 and 2.0017 ± 0.0005, respectively. The marginal difference is possibly due to bundling of nanotubes in the SWCNT sediment. The centrifuged supernatant shows negligible EPR signal with a similar *g*-factor of 2.0026 ± 0.0005 and line width of ~5.0 ± 0.1 G. We can deduce that the EPR signal is linked to the presence of catalyst particles present in the sonicated and sediment samples. DGU SWCNTs showed minimal EPR signal, further indicating that the observed EPR signal is related to the presence of catalyst particles. SWCNTs purified by aqua regia microwave digestion have been shown to contain catalyst particles through HRTEM (Figure 3a). Figure 5b shows the EPR signal of the aqua-regia-treated SWCNTs, which is similar to the signal of the sonicated and sediment catalyst containing SWCNTS, emphasizing the relationship between the catalyst particle impurities and EPR.

Figure 6a shows the observed EPR from Meijo SO SWCNTs, Meijo FHP, and refluxed Meijo FHP CNTs. Low

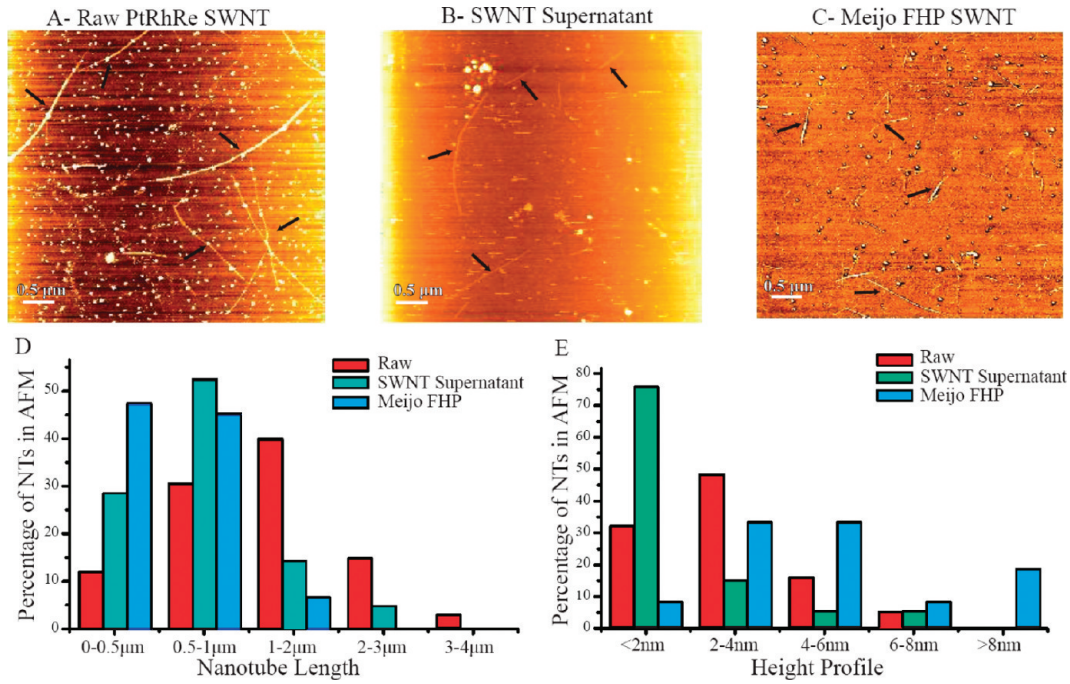

Figure 4. (A) AFM image of raw PtRhRe SWCNTs; (B) AFM image of SWCNTs supernatant; (C) AFM image of Meijo FHP nanotubes; (D) distribution of nanotube length for nanotube samples; (E) height profile distribution of nanotubes.

temperature (5 K) EPR measurements of Meijo SO SWCNTs show a large single peak with Lorentzian line shape and a *g*-factor of 2.0012 ± 0.0005 and ~5.1 ± 0.1 G line width. This EPR signal can be attributed to the presence of residual magnetic catalyst particles. Meijo FHP CNTs have negligible magnetic catalyst particle content and contain a combination of primarily

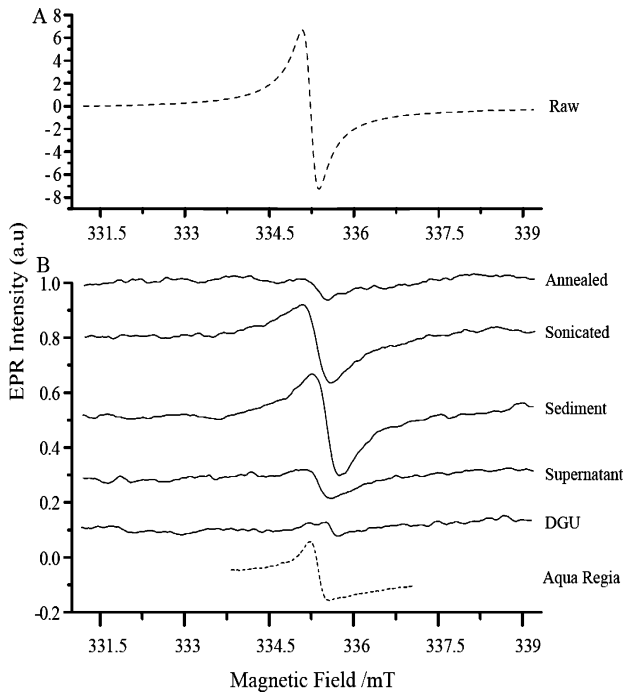

Figure 5. (A) 5 K EPR spectra of raw PtRhRe SWCNTs; (B) 5 K EPR spectra of annealed, sonicated, sediment, supernatant, DGU, and aqua regia SWCNTs (microwave power, 1 mW; modulation frequency, 100 kHz; modulation amplitude, 1 G).

SWCNTs and some double- and triple-walled nanotubes and show no observable EPR signal. This further supports the notion that the SWCNT EPR signals observed at X-band are linked to the presence of catalyst particles. Meijo FHP NTs are clean catalyst-free graphitic systems, differing from DGU SWCNTs as they are larger in diameter and contain double-walled and triple-walled nanotubes. Since no EPR signal is observed at the X-band for either nanotube sample, this suggests that changes in nanotube diameter and the number of walls do not produce an observable X-band EPR signal. Meijo FHP CNTs were refluxed to induce defects into the nanotube structure. The refluxed Meijo FHP CNTs showed no EPR signal at low temperature, similar to the raw Meijo FHP sample, indicating the minimal effect of defects on the EPR signal.

To further confirm the notion that ultrapure SWCNTs do not produce an observable signal in low temperature (5 K) EPR at X-band, we examined 95% purified semiconducting and 95% purified metallic SWCNT samples produced by Nanointegris using the DGU method.[12] No signal was observed from these samples as shown in Figure 6b. To our knowledge this is the first report of the EPR examination of pure metallic (and semiconducting) SWCNTs. This reveals that the EPR associated with possible conduction electrons is not seen at X-band and may require larger field strengths and higher microwave frequencies. This is highly challenging and is the subject of our further work.

Vibrating Sample Magnetometry. A vibrating sample magnetometer (VSM) was used to characterize the magnetic properties of the nanotube samples by measuring any magnetization arising from magnetic catalyst

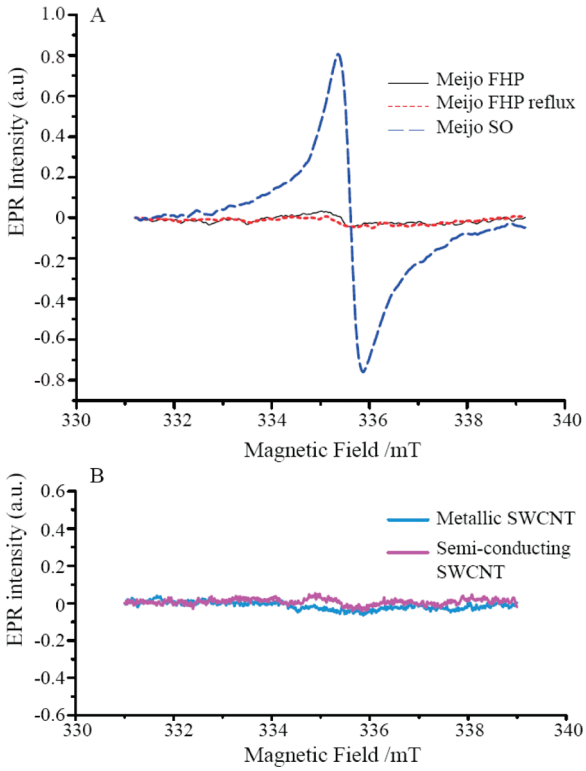

Figure 6. (A) The 5 K EPR of Meijo SO (dashed), Meijo FHP (solid), and refluxed Meijo FHP (dotted); (B) 5 K EPR of metallic SWCNT (blue) and semiconducting SWCNT (purple) (microwave power, 1 mW; modulation frequency, 100 kHz; modulation amplitude, 1 G).

particles and to further demonstrate that Meijo FHP nanotube were free from magnetic catalyst particles. Figure 7a shows the VSM of raw PtRhRe, Meijo FHP, and Meijo SO SWCNTs. The PtRhRe catalyst particles are nonmagnetic and therefore no magnetization curve is observed in the VSM. Meijo SO and FHP CNTs are synthesized using ferromagnetic catalysts, Ni/Y and Fe, respectively, and undergo high vacuum thermal annealing with the aim of removing catalyst particles.[16] Meijo SO SWCNTs are single-walled and have a similar diameter distribution to raw PtRhRe SWCNTs. The VSM of Meijo SO SWCNTs shows trace amounts of catalyst particles, as determined by the weak hysteresis curve. As a comparison, the inset in Figure 7a shows the VSM of Carbolex SWCNTs heavily coated with ferromagnetic catalyst particles; the strong hysteresis curve is indicative of the presence of soft magnetic catalyst particles (*cf.* ref 24). Meijo FHP nanotubes are of a larger diameter and contain single-walled and double-walled nanotubes. They are more stable to higher temperatures for annealing, resulting in maximum removal of magnetic catalyst particles; they therefore show no magnetic signals in VSM. These observations account for the origin of the detected EPR signal in Meijo SO SWCNTs, which contain magnetic catalyst particles, and the absence of any EPR signal for catalyst particle-free Meijo FHP NTs.

Raman Spectroscopy. Raman spectroscopy, shown in Figure 7b, was performed at 532 nm to measure the G and D peaks of the SWCNT samples to determine any effects the centrifugation purification process had upon SWCNT defects. The ratio of the D peak (~1330 cm^{-1}), defects in sp^2 carbon network, and the G peak (~1590 cm^{-1}), arising from semiconducting and metallic nanotubes, is used to measure the degree of disorder in the SWCNTs.[25] Similar D/G ratios were obtained for DGU SWCNTs, 0.059, and raw SWCNTs, 0.058, while smaller D/G ratios were obtained for aqua-regia-treated SWCNTs, 0.028, and Meijo SO SWCNTs, 0.032. The D peak for DGU SWCNTs may be slightly higher due to the horn-tip sonication process which may create defects through the process of cutting nanotubes. The relatively low D/G ratio for all the SWCNTs samples illustrates the high quality of the SWCNTs.[25,26]

Paramagnetic Properties. Purified DGU SWCNTs and Meijo FHP NTs free from catalyst particles show negligible EPR signals at X-band. EPR signals were only detected in samples containing catalyst particles indicating there may be some interactions between the metal catalyst and surrounding carbon which contributes to the EPR signal. Nicolau *et al.*[27] investigated the paramagnetic behavior of platinum catalyst deposited on charcoal. They investigated several compositions of platinum and charcoal and found that mixed Pt−C complexes produced EPR signals, with linewidths between 3.9 and 5.4 G and a *g*-factor of 2.0034, around that of a free electron and similar to the observed *g*-factors in Figures 5 and 6. The observed EPR signal was attributed to interaction between charcoal and the platinum, and a relationship between the EPR intensity and platinum content was observed, indicating that electrons remain unpaired on the platinum catalyst. These observations facilitate an understanding of the obtained EPR signals in our experiments. Annealing raw PtRhRe SWCNTs removes amorphous carbon surrounding the nanotube and catalyst particle surface. The cleansed catalyst particles no longer form Pt−C interactions with the removed amorphous carbon, explaining the absence of an observable EPR signal for annealed SWCNTs. Wang *et al.*[28] performed density functional theory (DFT) calculations to ascertain the binding energies of Pt clusters on carbon nanotubes. Binding energies on point defects on CNTs were determined to be more than three times higher than on defect-free CNTs. Stronger orbital hybridization between Pt atoms and carbon in defective CNTs was determined to cause the increase in the binding energy. Importantly Wang *et al.* elucidated that larger charge transfer occurred between Pt and carbon in defect CNTs. Sonication of SWCNT surfactant solution has been shown to cut nanotubes, and Lu *et al.* elucidated the mechanical damage that can potentially arise from ultrasonication, producing defects in the nanotube structure.[21,28,29] Shorter nanotubes with potential defects could provide more preferential binding sites

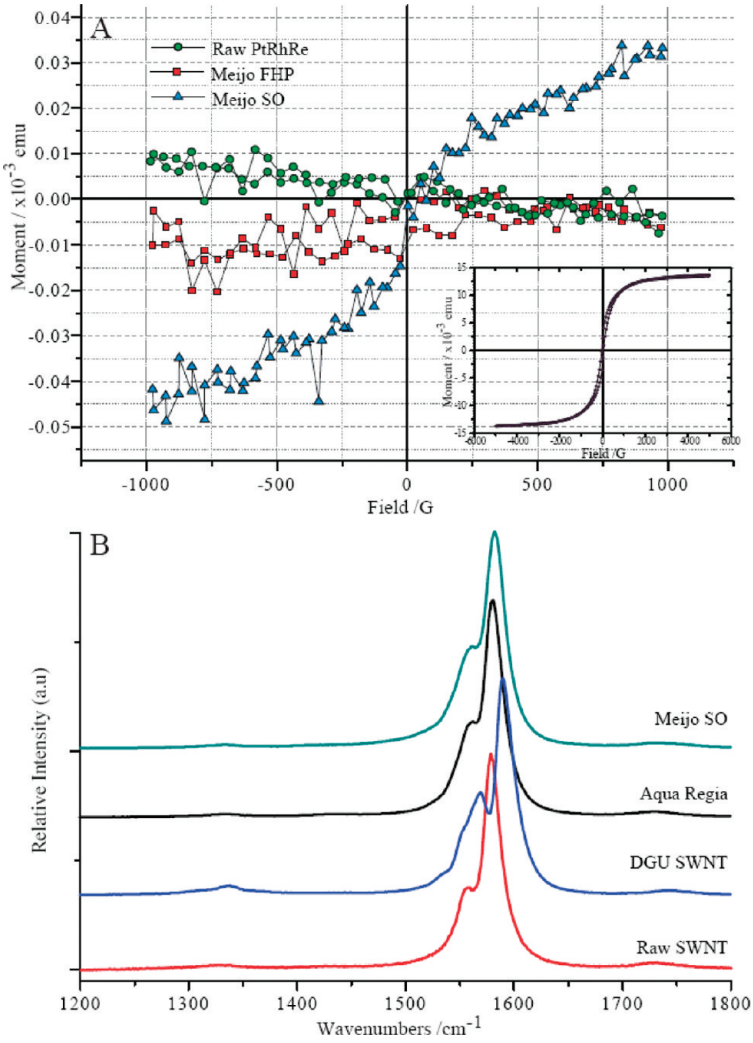

Figure 7. (A) VSM of raw PtRhRe (circle), Meijo FHP (square), and Meijo SO (triangle) SWCNTs. (Inset) VSM of Carbolex raw SWCNTs containing many catalyst particles. (B) Raman spectroscopy of Raw SWCNTs, DGU SWCNTs, aqua regia SWCNTs, and Meijo SO SWCNTs showing the G peak (~1590 cm^{-1}) and D peak (~1340 cm^{-1}).

for Pt catalyst particles to interact with the CNT and provide an explanation of the reappearance of an EPR signal for the sonicated SWCNTs sample. We centrifuged the sonicated SWCNT sample, producing two SWCNTs systems with varying Pt catalyst content, as determined by HRTEM. An EPR signal is observed for sediment SWCNTs, heavily coated with catalyst particles, due to the Pt−C interactions. Supernant and DGU SWCNTs, containing predominantly nanotubes, yielded no observable EPR signals at X-band due to the absence of Pt−C interactions. Observed EPR signals arise from the interaction between the Pt catalyst particle and the CNTs, and centrifugation has successfully demonstrated an avenue to reduce catalyst content from the nanotube system.[26,27] High vacuum thermal annealing of magnetic catalyst particles from Meijo FHP CNTs highlighted another approach to remove catalyst particles, which otherwise produce an EPR signal as seen for Meijo SO SWCNTs.[10,16] Meijo FHP CNTs have been shown to be a pure graphitic system, an ideal nanotube structure which has been lacking in preceding EPR studies, and shows no trace of conduction electrons. Theoretical calculations predict a doublet peak for SWCNTs EPR due to spin−charge separation; however, neither of our purified samples show this phenomenon at X-band.[30] Kuemmeth *et al.*[31] measured spin orbital coupling of 84 GHz for a single 5 nm diameter SWCNT.[31] On the basis of their measurement of the spin orbit (SO) coupling and theoretical study of ref 32, we can estimate a SO coupling for the nanotubes studied here (DGU SWCNTs diameter ≈ 1.4−1.6 nm, and Meijo FHP NTs, diameter ≈ 2 nm) to be approximately 260−300 GHz and 190−230 GHz, respectively. Given these values for SO coupling, we would expect no EPR signal from the conduction electrons at X-band (10 GHz) and at a modest magnetic field. Furthermore the range of nanotube diameters could lead to substantial broadening and therefore make it difficult to observe any signal. Studying aligned SWCNTs at higher EPR frequencies could reveal the conduction electron spin resonance.

SUMMARY

The multistep centrifugation purification process has successfully produced highly pure SWCNTs which can be implemented in spintronic devices. Centrifugation of SWCNT solutions provides an effective approach to removing catalyst particles compared to aqua regia treatment. HRTEM, UV−vis, and AFM provided evidence for the significant improvement of the SWCNTs through each step in the purification process. EPR tracked any modifications the purification methodology had on the SWCNTs sample. The comparative analysis of the sediment and supernatant SWCNT samples has revealed that metal catalyst carbon complexes were the cause of the observable EPR signal.

HRTEM and UV−vis established the difference between the two samples, the SWCNT sediment containing a substantial amount of catalyst particles and the SWCNT supernatant containing more isolated SWCNTs with considerable reduction in catalyst particle content and a narrower diameter distribution. EPR of the two contrasting SWCNT samples highlights a strong correlation between the level of catalyst particles and the detected EPR signal. Purified supernatant and DGU SWCNTs show no EPR signal at X-band, whereas the sonicated and sediment SWCNTs, containing higher levels of catalyst particles, both produced an EPR signal. Since aqua-regia-purified SWCNTs contain residual catalyst particles they therefore produce an EPR signal. Ultracentrifugation of raw PtRhRe is a viable method

to obtain catalyst-free SWCNTs. Meijo SO and FHP NTs illustrate analogous results. High thermal annealing of Meijo FHP NTs purged magnetic catalyst particles, as shown in VSM, whereas Meijo SO show the presence of magnetic particles in VSM. Meijo FHP nanotubes are highly pure, with HRTEM and VSM giving no indication of any catalyst particle present in the sample. The presence of catalyst particles in Meijo SO is demonstrated in the EPR in Figure 6a, with the magnetic catalyst-free Meijo FHP CNTs showing no EPR signal. Ultrapure DGU separated metallic and semiconducting SWNTs did not show any detectable EPR signal at the X-band either. We can conclude that in general high-quality ultrapure SWNTs do not exhibit an EPR signal at the X-band and that signals detected arise from metal catalyst particles interacting with carbon or in poor quality SWNT samples.

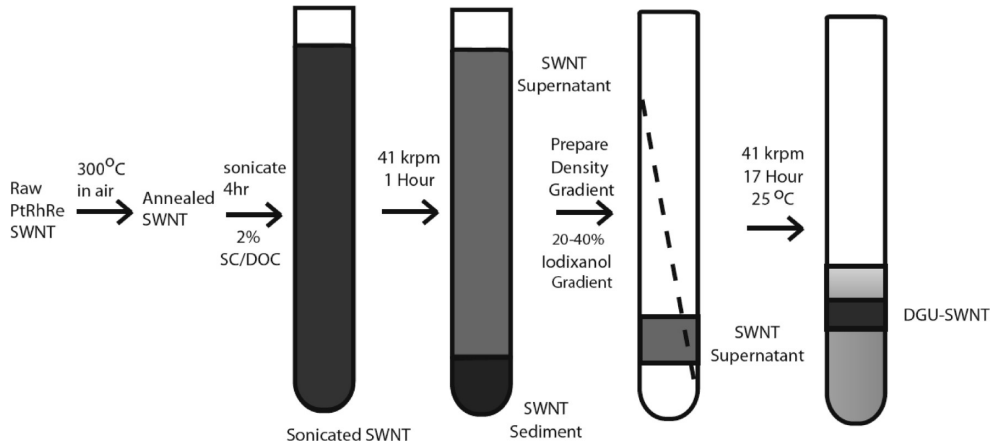

Figure 8. Schematic diagram indicating the multiple steps involved in the purification process of the SWCNTs.

METHODS

SWCNTs were grown using laser ablation with nonmagnetic catalyst particles (PtRhRe) using a previously reported method.[14] Purification to remove catalyst content was performed either by aqua-regia microwave digestion or through centrifugation.[15] Centrifugation involved multiple steps to purify the raw PtRhRe SWCNTs, as shown in the schematic diagram in Figure 8. The SWCNTs were annealed in air at 300 °C for 2 h in order to remove amorphous carbon. Annealed SWCNTs were dispersed in an aqueous solution of 2% sodium cholate (SC)/deoxy cholate (DOC) [ratio 4:1] to a concentration of 0.5 mg mL^{-1}. The SWCNT 2% SC/DOC solution was sonicated for 4 h using a horn-tip sonicator (Cole Parmer ultrasonic processor). The sample was placed in an ice bath to prevent thermal damage to the SWCNTs. The sonicated SWCNT solution was centrifuged for 1 h at 41 krpm using a swing bucket SW41Ti rotor and Beckman Coulter ultracentrifuge model L100-XP. The upper 85% of the solution was collected and is termed "SWCNT supernatant". The material at the bottom of the centrifuge tube was also collected and is termed "SWCNT sediment". The SWCNT supernatant was concentrated using centrifugal filters (Amicon 30 kDa, Millipore), for 7 min at 5 krpm, (Labofuge 200 Heraues). The concentrated SWCNT supernatant sample was further centrifuged for 17 h at 41 krpm using an iodixanol density gradient (20−40% linear gradient with 2% sodium cholate/sodium dodecyl sulfate [ratio 2:3]). The process of using density gradient ultracentrifugation (DGU) is employed with the primary function of isolating catalyst-free SWCNTs. The separated fractions from the DGU were isolated, and the bulk black nanotube suspension was collected and termed "DGU SWCNT". Meijo FHP and SO SWCNTs were produced by Meijo Nano Carbon, Inc, *via* arc-discharge using magnetic catalyst particles Fe and Ni/Y, respectively. As-grown arc-discharge SWCNTs were air oxidized at 400 °C and further purified in hydrochloric acid. High temperature annealing was performed between 1100−1400 °C at a vacuum pressure of 10^{-3}−10^{-4} Pa for 6−24 h. To understand the affect of nanotube defects on the EPR signal Meijo FHP SWCNTs were refluxed in nitric acid HNO_3 for 2.5 h at 130 °C in order to induce defects. DGU separated ultrapure semiconducting (IsoNanotube-S) and metallic (IsoNanotube-M) SWCNT buckypapers (95% purified) for EPR analysis were purchased from Nanointegris.

UV−vis absorption spectroscopy was measured for SWCNT films between 400 and 2200 nm using a Jasco V-570 UV/vis/NIR spectrometer. Vibration sample magnetometer measurements were performed using a Lakeshore 7400 VSM and EM4-HVA electromagnet. Atomic force microscopy (AFM) was performed using a Park Scientific instrument CP-II AFM. AFM samples were prepared by spin coating SWCNT solutions on functionalized Si/SiO substrates.[33] For high resolution transmission electron microscopy (HRTEM), SWCNT solutions were washed with methanol, and this washing repeated 5 times to ensure that the surfactant was removed. HRTEM was performed on a JEOL 4000EX operating at 80 kV. All samples for EPR were pumped to remove oxygen and sealed in a quartz tube under vacuum. EPR measurements were performed using a Bruker EMX spectrometer at 9.4 GHz at 5 K in an Oxford ESR900 cryostat. Raman spectroscopy was measured using a JY Horiba Labram Aramis Raman microscope using a frequency doubled Nd:YAG laser at 532 nm.

Acknowledgment. J.H.W. is supported by the Glasstone Fund and Brasenose College, Oxford. A.A. and J.J.L.M are supported by the Royal Society. G.A.D.B. thanks EPSRC, IMPRESS, (GR/S15808/01). M.H.R. thanks the EU (ECEMP) and the Freistaat Sachsen.

Supporting Information Available: UV−vis absorption of SWCNT films between 400−2200 nm. This material is available free of charge via the Internet at http://pubs.acs.org.

REFERENCES AND NOTES

1. Zutić, I.; Fabian, J.; Das Sarma, S. Spintronics: Fundamentals and Applications. *Rev. of Mod. Phys.* **2004**, *76*, 323–410.
2. Hueso, L. E.; Pruneda, J. M.; Ferrari, V.; Burnell, G.; Valdes-Herrera, J. P.; Simons, B. D.; Littlewood, P. B.; Artacho, E.; Fert, A.; Mathur, N. D. Transformation of Spin Information into Large Electrical Signals Using Carbon Nanotubes. *Nature* **2007**, *445*, 410–413.
3. Petit, P.; Jouguelet, E.; Fischer, J. E.; Rinzler, A. G.; Smalley, R. E. Electron Spin Resonance and Microwave Resistivity of Single-Wall Carbon Nanotubes. *Phys. Rev. B* **1997**, *56*, 9275–9278.

4. Bandow, S.; Asaka, S.; Zhao, X.; Ando, Y. Purification and Magnetic Properties of Carbon Nanotubes. *Appl. Phys. A* **1998**, *67*, 23–27.
5. Salvetat, J. P.; Feher, T.; L'Huillier, C.; Beuneu, F.; Forro, L. Anomalous Electron Spin Resonance Behaviour of Single-Walled Carbon Nanotubes. *Phys. Rev. B* **2005**, *72*, 075440.
6. Corzilius, B.; Gembus, A.; Weiden, N.; Dinse, K. P.; Hata, K. EPR Characterization of Catalyst-free SWNT and N@C_{60}-Based Peapods. *Phys. Stat. Sol. (b)* **2006**, *243*, 3273–3276.
7. Zaka, M.; Warner, J. H.; Ito, Y.; Morton, J. J. L.; Rümmeli, M. H.; Pichler, T.; Ardavan, A.; Shinohara, H.; Briggs, G. A. D. Exchange Interactions of Spin-Active Metallofullerenes in Solid-State Carbon Networks. *Phys. Rev. B.* **2010**, *81*, 075424.
8. Náfrádi, B.; Nemes, N. M.; Fehér, T.; Forró, L.; Kim, Y.; Fischer, J. E.; Luzzi, D. E.; Simon, F.; Kuzmany, H. Electron Spin Resonance of Single-Walled Carbon Nanotubes and Related Structures. *Phys. Stat. Sol. (b)* **2006**, *243*, 3106–3110.
9. Shen, K.; Tierney, D. L.; Pietraβ, T. Electron Spin Resonance of Carbon Nanotubes Under Hydrogen Adsorption. *Phys. Rev. B.* **2003**, *68*, 165418.
10. Kitaura, R.; Ogawa, D.; Kobayashi, K.; Saito, T.; Ohshima, S.; Nakamura, T.; Yoshikawa, H.; Awaga, K.; Shinohara, H. High Yield Synthesis and Characterization of the Structural and Magnetic Properties of Crystalline $ErCl_3$ Nanowires in Single-Walled Carbon Nanotube Templates. *Nano Res.* **2008**, *2*, 152–157.
11. Nishide, D.; Miyata, Y.; Yanagi, K.; Tanaka, T.; Kataura, H. Effective Separation of Carbon Nanotubes and Metal Particles from Pristine Raw Soot by Ultracentrifugation. *Jpn. J. Appl. Phys.* **2009**, *48*, 015004.
12. Arnold, M. S.; Green, A. A.; Hulvat, J. F.; Stupp, S. I.; Hersam, M. C. Sorting Carbon Nanotubes by Electronic Structure using Density Differentiation. *Nat. Nanotechnol.* **2006**, *1*, 60–65.
13. Yanagi, K.; Miyata, Y.; Kataura, H. Optical and Conductive Characteristics of Metallic Single-Wall Carbon Nanotubes with Three Basic Colors; Cyan, Magenta, and Yellow. *Appl. Phys. Exp.* **2008**, *1*, 034003.
14. Rümmeli, M. H.; Kramberger, C.; Löffler, M.; Jost, O.; Bystrzejewski, M.; Grüneis, A.; Gemming, T.; Pompe, W.; Büchner, B.; Pichler, T. Catalyst Volume to Surface Area Constraints for Nucleating Carbon Nanotubes. *J. Phys. Chem. C* **2007**, *111*, 8234–8241.
15. Schönfelder, R.; Rümmeli, M. H.; Gruner, W.; Löffler, M.; Acker, J.; Hoffmann, V.; Gemming, T.; Büchner, B.; Pichler, T. Purification-Induced Sidewall Functionalization of Magnetically Pure Single-Walled Carbon Nanotubes. *Nanotechnology* **2007**, *18*, 375601.
16. Zhao, X.; Inoue, S.; Jinno, M.; Suzuki, T.; Ando, Y. Macroscopic Oriented Web of Single-Wall Carbon Nanotubes. *Chem. Phys. Lett.* **2003**, *373*, 266–271.
17. Hu, H.; Zhao, B.; Itkis, M. E.; Haddon, R. C. Nitric Acid Purification of Single-Walled Carbon Nanotubes. *J. Phys. Chem. B* **2003**, *107*, 13838–13842.
18. Kataura, H.; Kumazawa, Y.; Maniwa, Y.; Umezu, I.; Suzuki, S.; Ohtsuka, Y.; Achiba, Y. Optical Properties of Single-Wall Carbon Nanotubes. *Synth. Met.* **1999**, *103*, 2555–2558.
19. Itkis, M. E.; Perea, D. E.; Niyogi, S.; Rickard, S. M.; Hamon, M. A.; Hu, H.; Zhao, B.; Haddon, R. C. Purity Evaluation of As-Prepared Single-Walled Carbon Nanotube Soot by Use of Solution-Phase Near-IR Spectroscopy. *Nano Lett.* **2003**, *3*, 309–314.
20. Yudasaka, M.; Zhang, M.; Jabs, C.; Iijima, S. Effect of an Organic Polymer in Purification and Cutting of Single-Wall Carbon Nanotubes. *Appl. Phys. A* **2000**, *71*, 449–451.
21. Shelimov, K. B.; Esenaliev, R. O.; Rinzler, A. G.; Huffman, C. B.; Smalley, R. E. Purification of Single-Wall Carbon Nanotubes by Ultrasonically Assisted Filtration. *Chem. Phys. Lett.* **1998**, *282*, 429–434.
22. Cantone, A. L.; Buitelaar, M. R.; Smith, C. G.; Anderson, D. G.; Jones, A. C.; Chorley, S. J.; Casiraghi, C.; Lombardo, A.; Ferrari, A. C.; Shinohara, H.; *et al.* Electronic Transport Characterization of Sc@C_{82} Single-Wall Carbon Nanotube Peapods. *J. Appl. Phys.* **2008**, *104*, 083717.
23. Asada, Y.; Miyata, Y.; Ohno, Y.; Kitaura, R.; Sugai, T.; Mizutani, T.; Shinohara, H. High-Performance Thin-Film Transistors with DNA-Assisted Solution Processing of Isolated Single-Walled Carbon Nanotubes. *Adv. Mater.* **2010**, *22*, 2698–2701.
24. Schäffel, F.; Täschner, C.; Rümmeli, M. H.; Neu, V.; Wolff, U.; Queitsch, U.; Pohl, D.; Kaltofen, R.; Leonhardt, A.; Rellinghaus, B.; *et al.* Carbon Nanotubes Terminated with Hard Magnetic FePt Nanomagnets. *Appl. Phys. Lett.* **2009**, *94*, 193107.
25. Eklund, P. C.; Holden, J. M.; Jishi, R. A. Vibrational Modes of Carbon Nanotubes; Spectroscopy and Theory. *Carbon* **1995**, *33*, 959–972.
26. Dennany, L.; Sherrell, P.; Chen, J.; Innis, P. C.; Wallace, G. G.; Minett, A. I. EPR Characterisation of Platinum Nanoparticle Functionalised Carbon Nanotube Hybrid Materials. *Phys. Chem. Chem. Phys.* **2010**, *12*, 4135–4141.
27. Nicolau, C. S.; Thom, H. G.; Pobitschka, E. Electron Spin Resonance Studies of some Supported Hydrogenation−Dehydrogenation Catalysts. *Trans. Faraday Soc.* **1959**, *55*, 1430–1434.
28. Wang, J.; Lv, Y.; Li, X.; Dong, M. Point-Defect Mediated Bonding of Pt Clusters on (5,5) Carbon Nanotubes. *J. Phys. Chem. C.* **2009**, *113*, 890–893.
29. Lu, K. L.; Lago, R. M.; Chen, Y. K.; Green, M. L. H.; Harris, P. J. F.; Tsang, S. C. Mechanical Damage of Carbon Nanotubes by Ultracentrifugation. *Carbon* **1996**, *34*, 814–816.
30. De Martino, A.; Egger, R.; Hallberg, K.; Balseiro, C. A. Spin-Orbit Coupling and Electron Spin Resonance Theory for Carbon Nanotubes. *Phys. Rev. Lett.* **2002**, *88*, 206402.
31. Kuemmeth, F.; Ilani, S.; Ralph, D. C.; McEuen, P. L. Coupling of Spin and Orbital Motion of Electrons in Carbon Nanotubes. *Nature* **2008**, *452*, 448–452.
32. Huertas-Hernando, D.; Guinea, F.; Brataas, A. Spin-Orbit Coupling in Curved Graphene, Fullerenes, Nanotubes, and Nanotube Caps. *Phys. Rev. B* **2006**, *74*, 155426.
33. Liu, J.; Casavant, M. J.; Cox, M.; Walters, D. A.; Boul, P.; Lu, W.; Rimberg, A. J.; Smith, K. A.; Colbert, D. T.; Smalley, R. E. Controlled Deposition of Individual Single-Walled Carbon Nanotubes on Chemically Functionalized Templates. *Chem. Phys. Lett.* **1999**, *303*, 125–129.